

# Gapless 3D Topological Insulator Based on Partially Relaxed HgTe Film

M. L. Savchenko,<sup>1,2</sup> D. A. Kozlov,<sup>1,2</sup> N. N. Vasilev,<sup>1,2</sup> Z. D. Kvon,<sup>1,2</sup>  
N. N. Mikhailov,<sup>1,2</sup> S. A. Dvoretzky,<sup>2</sup> and A. V. Kolesnikov<sup>2</sup>

<sup>1</sup>*Novosibirsk State University, Novosibirsk 630090, Russia*

<sup>2</sup>*Rzhanov Institute of Semiconductor Physics, Novosibirsk 630090, Russia*

(Dated: April 6, 2022)

Surface states of topological insulators (TIs) played the central role in the majority of outstanding investigations in low-dimensional electron systems for more than 10 years. But it is still an open question how the properties of these states depend on the trivial carriers existence and if they survive at all if a bulk energy gap collapses. In this work, by combining transport measurements together with capacitance spectroscopy we have performed the analysis of a 200 nm partially relaxed HgTe film. The Drude fit of classical magnetotransport revealed the ambipolar electron-hole transport with high electron mobility. The detailed analysis of Shubnikov-de Haas oscillations both in conductivity and capacitance distinguished three groups of electrons identified as electrons on the top and bottom surfaces and the bulk electrons. The value of the bulk energy gap is found to be close to zero. It has been established that the absence of the gap does not affect the surface states which are found to be well-resolved and spin non-degenerated. The results of the work confirm that the topological surface states are robust to the absence of the bulk gap. Presented techniques allows to investigate other 3D TIs regardless of the bulk conductance existence.

## I. INTRODUCTION

An ideal three dimensional topological insulator (3D TI) is a system that has spin non-degenerate surface states with spin-momentum locking and insulating bulk [1]. The unique properties of 3D TIs result in many new physical effects: spin polarization of 3D TI current [2],  $4\pi$  oscillations in superconductor contact [3], universal magnetoelectric effect [4], Majorana fermions [5]. The existence of surface states are established in Bi-, Sb-based and HgTe 3D TIs by means of ARPES [6–9], and then studied by magneto-optic [4, 10, 11], transport methods [9, 12–15] and magnetocapacitance spectroscopy [16].

There are several issues hampering the investigation of surface states. The main shortcoming of Bi- and Sb-based 3D TIs is a crystalline imperfection leading to intrinsic doping and reduced carriers mobility. Quite recently even fabrication of samples with pure surface conductivity was difficult to implement and one has to study either transport response of surface states intermixed with the bulk one [17–20] or to use other techniques e.g. studying photogalvanics effects involving space symmetry analysis [21] allowing to distinguish bulk and surface carriers. In recent papers the surface-dominant conductivity was conclusively shown [22–25], though even the best samples still have significant disorder, smearing of fine effects: for instance, pronounced QHE plateaux requires a magnetic field close to the limit of superconductive magnets or even exceeding it [23–25].

In contrast, HgTe-based 3D TIs are characterized by much smaller disorder and higher values of electron mobility exceeding  $10^5 \text{ cm}^2/\text{V}\cdot\text{s}$  [14]. The highest quality of the system even allowed to study delicate ballistic and interference effects [15, 26]. However, such system has its own shortcomings mainly coming from the fact of zero energy gap in bulk HgTe. In order to open a gap and organize 3D TI one has to apply a strain: HgTe

films, grown on CdTe substrate with 0.3% lattice mismatch have a gap of just 15 meV. In turn, the requirement of strain limits the maximum thickness of HgTe film by about 100-150 nm (according to [9] and our experience) because of relaxation at higher thicknesses. This fact explains why in the majority of papers devoted to HgTe-based 3D TIs only 70-100 nm films were studied [3, 9, 14, 15, 26–29]. On the other hand, studying of thicker HgTe films also consists of interest because of higher separation between surface states, weaker mutual electrostatic connection and possible hybridization. One could expect that thicker films should be partially or fully relaxed resulting in smaller or even zero energy gap. In such system the bulk carriers will inevitably appear on every position of the Fermi level. With a view to foregoing, the issue of surface and bulk states coexistence seems to be actual. Moreover, some of new predicted materials with non-trivial topology do not have a band gap or are semimetals [30, 31].

In this paper we investigate a 200 nm HgTe film that could be characterized by partial strain and almost zero bulk energy gap. The samples under investigations are equipped with a metallic gate allowing to widely vary a Fermi level position from the valence band to the conduction one. By combining a traditional classical and quantum magnetotransport study as well as magnetocapacitance spectroscopy we show that both zero gap and the presence of trivial bulk conductivity does not affect the surface states. By detailed analysis we reveal the main properties of the surface and bulk carriers and prove that the surface states are still spin non-degenerated.

## II. EXPERIMENTAL DETAILS

All measurements are carried out on 200 nm HgTe films that have been grown by molecular beam epitaxy on

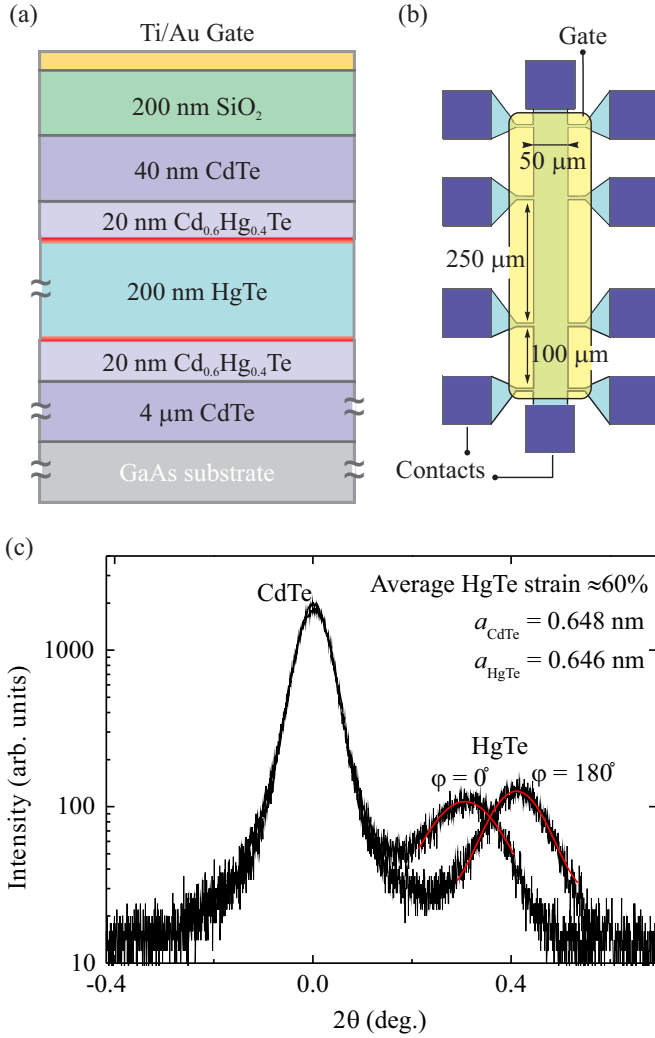


FIG. 1. (a) The schematic cross-section of the structure under study. The 200 nm HgTe film is sandwiched between thin  $\text{Cd}_{0.6}\text{Hg}_{0.4}\text{Te}$  buffer layers, covered by a 200 nm  $\text{SiO}_2$  insulator and a metallic gate. Bright red lines represent the surface states on the top and bottom surfaces of the film. (b) The schematic top view of studied Hall-bars. (c) X-ray diffraction curves of the system obtained in the opposite directions for the  $[026]$  reflex (for the azimuth angle  $\varphi = 0^\circ$  and  $180^\circ$ ). Relative to CdTe, the positions of HgTe peaks allow to determine its average strain that is about 60% (100% means that HgTe film has the lattice constant of CdTe and a 15 meV bulk band gap, 0% means that it is fully relaxed to its own lattice constant and has some meV of the bands overlap [32]).

GaAs(013) substrate with the same layers ordering as it was for usual 80 nm films [14].

Fig. 1(a) schematically shows the cross-section view of the system under study. The 200 nm HgTe film is sandwiched between thin  $\text{Cd}_{0.6}\text{Hg}_{0.4}\text{Te}$  barriers, a Ti/Au gate has been deposited on 200 nm  $\text{SiO}_2$  insulator grown by low temperature chemical vapor deposition.

An approximate thickness of pseudomorphic growth of HgTe film on the CdTe substrate with 0.3% larger lat-

tice constant is about 100 – 150 nm (according to [9] and our experience). The full 100% strain of HgTe in this conditions results in an indirect 15 meV bulk band gap [10]. To reveal the crystalline perfection of the grown 200 nm HgTe structure a two-crystal X-ray diffractometer was used ( $\text{Cu-K}\alpha$  radiation, a Ge (400) monochromator). Fig. 1(c) shows the high resolution diffraction curves of  $[026]$  reflex in a symmetrical Bragg geometry. The data confirm the suggested relaxation, but not full – the structure still has about 60% strain. It means that on average the structure has less than 15 meV a band gap (following transport measurements show nearly zero band gap existence).

Several Hall-bar samples have been prepared from one wafer showing similar results. For conformity of magnetotransport and capacitance responses comparison of all the data presented obtained from one sample. Fig. 1(b) shows the schematic top view of the studied Hall-bars with a  $50\ \mu\text{m}$  current channel and equal to 100 and  $250\ \mu\text{m}$  distances between potential probes. Transport measurements were performed using a standard lock-in technique with driving currents in the range of  $10^{-7}$  –  $10^{-8}$  A in the perpendicular magnetic field  $B$  up to 12 T at the temperature 0.2 K. A typical frequency for transport measurements was 12 Hz that was decreased to 2 Hz in the case of high-magnetic fields. For the capacitance measurements we superimpose the dc bias  $V_g$  with a small ac voltage  $V_{ac}$  and measure the ac current flowing across our device phase sensitively. The total capacitance measured in such way between a metallic top gate and a 2D electron system (2DES) depends, besides the geometric capacitance, on the quantum capacitance  $e^2D$ , connected in series and reflecting the finite density of states  $D$  of the 2DES [16, 33];  $e$  is the elementary charge,  $D$  is thermodynamic density of states. The ac frequency for capacitance measurements was in the range of 2 – 680 Hz. The frequency independence of measured resistance and capacitance  $C$  has been controlled excluding both the existence of leakage currents and resistive effects. The parasitic capacitance of our set up is about 40 pF.

### III. RESULTS AND DISCUSSION

The detailed analysis of the magnetotransport and capacitance data reveals the following main idea: the spin non-degenerate surface states, originated from the inverted band structure of HgTe, persists in 200 nm partially relaxed film and act in a very similar way as in strained films with bulk gap. Like it is for 80 nm HgTe films [14, 16], the surface carriers of the system are high mobility electrons, while in the bulk one could observe both electrons and holes depending on the Fermi level position with virtually no energy bulk gap.

The inset of Fig. 2(a) shows the schematic suggested band diagram of the system at zero gate voltage. In terms of band structure, the partially relaxed 200 nm film behaves like an intermediate between 80 nm film [14] and

bulk HgTe [32]. While the conduction band has its minimum at  $\Gamma$  point, the top of the valence band is situated on aside of Brillouin zone center with an indirect energy bulk gap around 3 meV. The band inversion symmetry of the system results in the formation of the topological surface states [1] (shown in red in Fig. 2 (a)) with linear-like dispersion and a Dirac point located deep in the valence band [9].

### A. Classical transport and Drude fitting

Figure 2(a) shows the typical resistivity  $\rho_{xx}$  at magnetic field  $B = 0$  and Hall resistance  $\rho_{xy}$  at  $B = 0.5$  T as a function of gate voltage  $V_g$  at  $T = 0.2$  K. The  $\rho_{xx}$  trace exhibits a maximum near  $V_g = 1$  V and is asymmetric with respect to  $V_g$ : the resistance on the left-hand side of the maximum is significantly higher than on the right side. In the vicinity of  $V_g = 1$  V point the  $\rho_{xy}$  changes its sign. The obtained behavior is very similar to observed in thinner HgTe films [14] and inline with the expectations that the gate voltage changes the position of the Fermi level from the valence band to the conduction one. On the right-hand side from the peak, where  $\rho_{xy}$  is negative, the Fermi level goes to the conduction band and the carriers are high-mobility surface electrons and moderate-mobility bulk ones. In this region the  $\rho_{xx}$  reaches its minimal values. At negative gate voltages the Fermi level goes to the valence band, where bulk holes and surface electrons coexist resulting in non-linear sign-variable Hall effect similar to what was observed in 80 nm films [14] (not shown). An almost one order difference in  $\rho_{xx}$  values between left- and right-hand sides of the resistivity peak indicates to significant difference in electron and hole mobilities.

In order to obtain the values of electron and hole densities and mobilities ( $n_{\text{Drude}}$  and  $p_{\text{Drude}}$ ,  $\mu_e$  and  $\mu_p$  correspondingly) we used the two-component Drude model fitting of both  $\rho_{xx}(B)$  and  $\rho_{xy}(B)$  dependencies at fixed gate voltages, as it were carried out in our former works [14, 34]. One should note that practically there are more than one kind of electrons are present in the system, namely: two kinds of surface electrons (from the top and bottom surfaces) and bulk carriers. However, the tolerance of Drude model does not allow to distinguish between them. Therefore the values of  $n_{\text{Drude}}$  and  $\mu_e(V_g)$ , obtained from fitting, reveals the total electron density and their average mobility. The obtained by this manner  $n_{\text{Drude}}(V_g)$  and  $p_{\text{Drude}}(V_g)$  density dependencies are shown in Fig. 2 (b). The mobility dependence  $\mu_e(V_g)$  for region  $V_g > 0$  is shown in the inset. At the negative gate voltage side, where bulk holes and surface electrons coexist, the fitting performed provides both densities but only hole mobility, while the electron mobility stays uncertain. The hole mobility is proved to be gate independent and has value of about  $10^4$  cm<sup>2</sup>/Vs (not shown).

The density dependencies obtained from Drude fitting could be interpreted by the following way. At zero gate

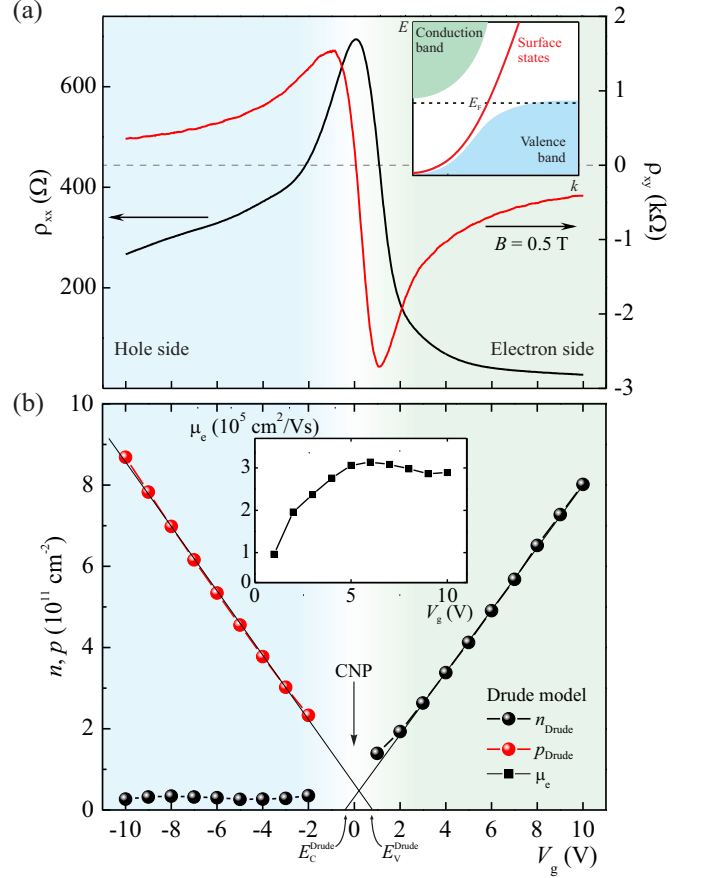


FIG. 2. (a) The gate dependencies of longitudinal  $\rho_{xx}$  (measured at zero magnetic field, a black line) and Hall resistances  $\rho_{xy}$  (at magnetic field  $B = 0.5$  T, a red line).  $\rho_{xx}$  exhibits its maximum while  $\rho_{xy}$  changes the sign in the vicinity of charge neutrality point (CNP) of the system. *Inset* – the schematic band diagram of the system at zero gate voltage. (b) The gate voltage dependencies of the total electron  $n_{\text{Drude}}$  (black spheres) and hole  $p_{\text{Drude}}$  (red spheres) densities, obtained from two-component Drude model fitting of  $\rho_{xx}(B)$  and  $\rho_{xy}(B)$  traces. The linear extrapolation of  $p_{\text{Drude}}$  and  $n_{\text{Drude}}$  to zero values results in highlighting of two points on the  $V_g$ -axis for holes and electrons, accordingly, marked as  $E_V^{\text{Drude}}$  at  $V_g \approx 0.8$  V and  $E_C^{\text{Drude}}$  at  $V_g \approx -0.3$  V. The first point corresponds to the state of the system when the Fermi level touches the top of the valence band. However, the second point has only the virtual meaning without any well-defined state of the system (see text for the details). *Inset* – the gate dependence of the average electron mobility  $\mu_e$  at positive gate voltages.

voltage the Fermi level is located near the top of the valence band, where the bulk holes coexist with nearly the same number of electrons, presumably the surface ones. By applying a small positive  $V_g$  one increases the total electron density  $n_{\text{Drude}}(V_g)$  though not with the full filling rate because of the bulk hole presence. At  $V_g = E_V^{\text{Drude}}$  (see the caption for fig. 2) the Fermi level touches the top of the valence band. At  $V_g > E_V^{\text{Drude}}$  the bulk holes disappear while the electron density  $n_{\text{Drude}}$  in-

creases linearly with  $V_g$  with the full filling rate. On the contrary, by applying a negative  $V_g$  one mainly increases  $p_{\text{Drude}}$ , while  $n_{\text{Drude}}(V_g)$  stays almost constant because of much smaller values of effective mass and so the density of states. A small increase of  $n_{\text{Drude}}(V_g)$  observed at  $V_g < -5$  V has no physical sense and probably indicates to a fitting uncertainty in this range. The total filling rate  $dn/dV_g$  describes the change of the total carrier charge density ( $n_{\text{Drude}} - p_{\text{Drude}}$ ) with  $V_g$  and mainly determined by the insulator layers sequence. The obtained from experiment filling rate is found to be  $8.0 \times 10^{10} \text{ cm}^{-2}/\text{V}$  which is in line with electrostatic calculations.

One should note that Drude fitting gives only the total electron density value and not the partial ones. Since that Drude fitting does not reveal the actual position of the bottom of the conduction band. The obtained from linear extrapolation  $E_C^{\text{Drude}}$  point on  $V_g$ -axis does not correspond to any well-defined state of the system and has only virtual sense. Therefore it is impossible to extract the bulk energy gap value from classical magnetotransport data. More information could be obtained only from the quantum oscillations analysis.

### B. Quantum Transport and Capacitance Oscillations

In contrast to the classical transport the analysis of Shubnikov-de Haas (SdH) oscillations in a systems with high enough quantum mobility allows to determine the partial densities of all carriers [14, 35]. One could expect four groups of carries in the system under study, though at  $V_g > E_V^{\text{Drude}}$  only three of them rest. Each group of carriers is characterized by a density giving its own frequency of SdH oscillations in  $1/B$  scale. The issue of carriers identification from the resistivity oscillations with three kinds of electrons in a general case looks rather complicated and its solution is too ambiguous. On the other hand, the issue could be simplified if one complements the resistivity oscillations with the capacitance ones. In a case of an ordinary 2DES the capacitance oscillations simply reflects the density of states modulation by magnetic field. However, in a case of essentially thick film with several group of carriers which are located at different areas across the film it turns out that the amplitude of capacitance oscillations produced from each group gets the inverse relation with a distance from the carriers of the group to the gate [16, 36]. Therefore one could expect that the amplitude of SdH oscillations observed in capacitance induced by the top surface electrons should be enhanced at most while the electrons on the bottom surface, as the most distant from the gate, will produce oscillations of suppressed amplitude. By comparison the oscillations in capacitance and transport and their Fourier spectra, measured in the same conditions, one could identify who is who.

Fig. 3 shows normalized SdH conductivity oscillations  $\Delta\sigma_{xx}/\sigma_{xx}^0$  at different gate voltages (panels (a) and (b))

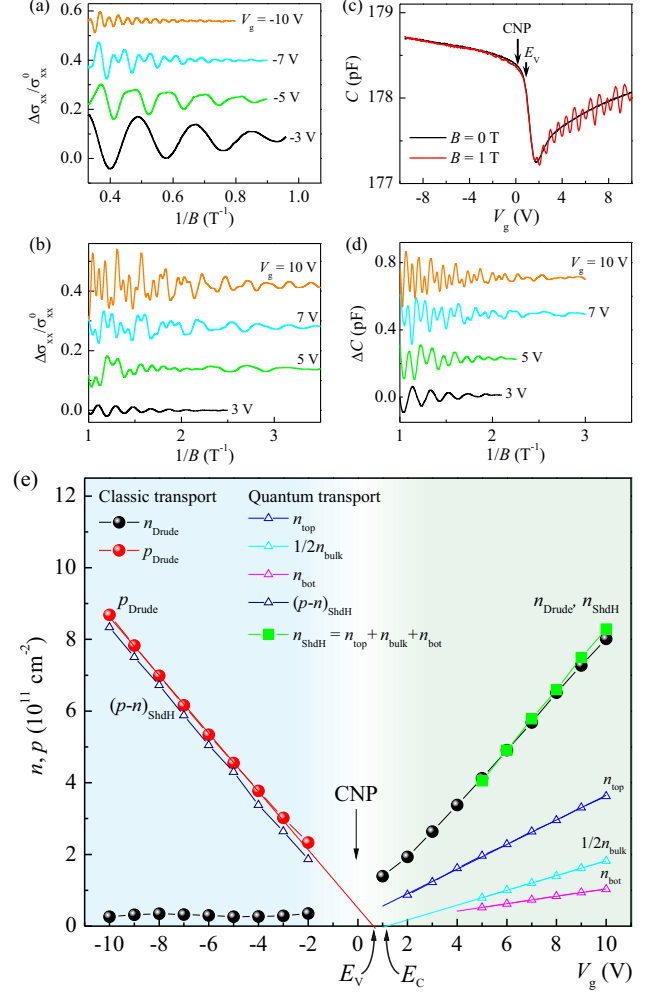


FIG. 3. (a), (b) The normalized conductivity oscillations  $\Delta\sigma_{xx}/\sigma_{xx}^0 = (\sigma_{xx} - \langle \sigma_{xx} \rangle) / \sigma_{xx}^0$  in  $B^{-1}$  scale for the hole and electrons sides, respectively, where  $\langle \sigma_{xx} \rangle$  denotes monotonous part of  $\sigma_{xx}$  and  $\sigma_{xx}^0 \equiv \sigma_{xx}(B=0)$ . (c) The gate dependencies of capacitance  $C(V_g)$  measured at zero magnetic field (a black line) and at  $B = 1$  T (a red line). (d) The SdH oscillations in  $\Delta C = C - C(B=0)$  for the electron side. (e) The combined gate voltage density dependencies obtained from both classical transport and SdH oscillations analysis. Presented above in the Fig. 2 (b)  $n_{\text{Drude}}$  and  $p_{\text{Drude}}$  has the same color code and shown in black and red spheres, respectively. From SdH oscillations the following densities were obtained: the differential density  $(p-n)_{\text{SdH}}$  for the hole side, and partial densities  $n_{\text{top}}$ ,  $n_{\text{bulk}}$  and  $n_{\text{bot}}$  for the electron side. For the consistency with FFT spectra analysis, the  $1/2 \cdot n_{\text{bulk}}$  is shown. Also the total electron density, obtained as  $n_{\text{SdH}} = n_{\text{top}} + n_{\text{bulk}} + n_{\text{bot}}$  shown in green squares.

vs reciprocal magnetic field  $B^{-1}$ , gate dependence of measured capacitance  $C(V_g)$  at zero and non-zero magnetic field (c) and its oscillations  $\Delta C(B^{-1})$  for different  $V_g$  values (d). Each oscillation pattern in  $B^{-1}$  scale was subject to fast Fourier transform (FFT) analysis (see Appendixes for details).

On the hole side of the gate voltages the SdH oscilla-



tions (Fig. 3 (a)) demonstrate the simplest pattern and their Fourier spectra demonstrate two well-defined peaks (see Fig. 4 (a)). The behavior is typical for 2D systems, where high-mobility and low-density electrons coexist with low-mobility and high-density holes. Because of low density, the electrons do not produce any well-resolved peak on Fourier spectrum. On the contrary, the holes induces SdH oscillations accompanied with two well-resolved peaks on FFT spectrum of frequencies  $f_1^h$  and  $f_2^h$ . For every gate voltage these frequencies are governed by the relation  $2 \cdot f_1^h = f_2^h$  (see Fig. 4 (b)) and therefore correspond to a formation of spin-degenerated and spin-resolved bulk holes Landau levels accordingly. However, the exact frequency values correspond to the differential density ( $p - n$ ) and not to the hole's one [14, 37]. The gate voltage dependence of  $(p - n)_{\text{SdH}}(V_g) = 2e/h \cdot f_1^h$  is shown as blue triangles in Fig 3 (e). The obtained data is in full agreement with Drude fitting since it is clearly seen that  $(p - n)_{\text{SdH}}(V_g)$  dependence accurately follows  $p_{\text{Drude}}(V_g)$  with the shift of around  $n_{\text{Drude}}(V_g)$ , i.e.  $p_{\text{Drude}}(V_g) - n_{\text{Drude}}(V_g) = (p - n)_{\text{SdH}}(V_g)$ .

On the positive gate voltage side the SdH oscillations demonstrate much more complicated structure both in conductivity and capacitance (see Fig. 3 (b) and (d)). Since the high electron mobility the first oscillations appear at magnetic fields as low as 0.25 T while at  $B > 1$  T the transition to the quantum Hall state begins (not shown). Because of our focus on SdH oscillations we limited the magnetic field range to 1 T. For the traces measured at  $V_g \geq 5$  V the Fourier spectra demonstrate 3 well-resolved peaks (see Fig. 4 (a)), characterized by frequencies of  $f_1^e$ ,  $f_2^e$  and  $f_3^e$ , which are not multiple of each other. Also the additional peaks with the frequencies of  $f_i^e \pm f_j^e$  and of much smaller amplitude are seen. The comparison of the conductivity and capacitance Fourier spectra reveals that the relative peaks' height significantly differs between two techniques: the peak with frequency of  $f_3^e$  is strongly enhanced in capacitance spectra, which points out that it stems from top surface electrons with the density of  $n_{\text{top}} = e/h \cdot f_3^e$  (see Fig. 3 (e)), where  $e$  – is the electron charge,  $h$  – is Planck constant. On the contrary, the peak of  $f_1^e$  frequency is strongly suppressed in capacitance response indicating that it origins from the bottom surface electrons with the density of  $n_{\text{bot}} = e/h \cdot f_1^e$ . Then, the rest peak with the frequency of  $f_2$  should be associated with the bulk electrons. Since the bulk electrons are expected to be spin-degenerated then their density should be governed by the relation  $n_{\text{bulk}} = 2e/h \cdot f_2^e$ . One should note that the spin degeneracy of bulk carriers should be removed in strong magnetic fields. Indeed, the SdH oscillations splitting was observed in magnetic fields up to 5-12 T, but the corresponding Fourier spectra do not demonstrate well resolved peak with the frequency of  $2 \cdot f_2^e$  probably because of the proximity to  $f_3^e$  peak. At  $V_g < 5$  V the peaks with frequencies of  $f_1^e$  and  $f_2^e$  become hardly visible, while  $f_3^e$  peak persists.

An independent proof of supposed carriers identification could be obtained by comparison of densities, ob-

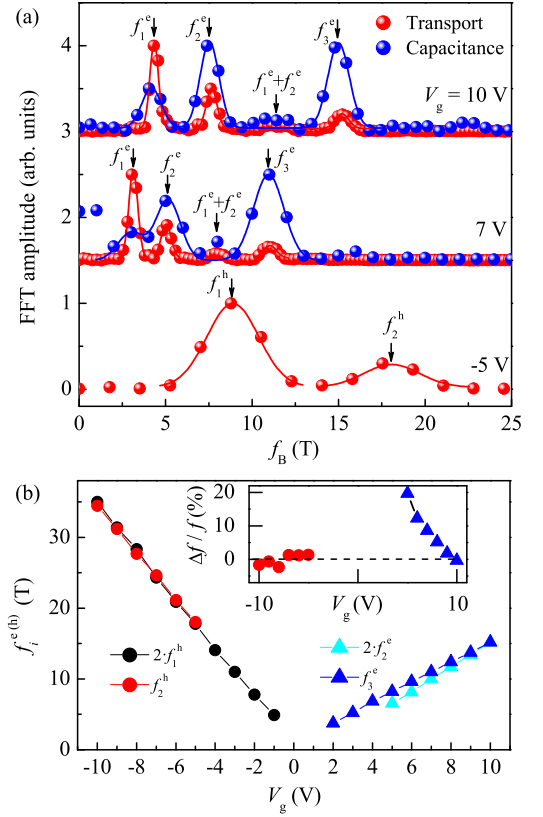


FIG. 4. (a) The typical Fourier spectra of conductivity (red spheres) and capacitance (blue spheres) of SdH oscillations at different fixed gate voltages. Solid lines correspond to the fitting by a Gaussian function. The vertical arrows point out to the central frequency of each Gaussian fit. (b) The ratio between positions of different peaks. On the hole side  $2 \cdot f_1^h(V_g)$  (black circles) closely follows the  $f_2^h(V_g)$  (red circles) dependence indubitably pointing to their common origin, namely spin-degenerated and spin-resolved Landau levels of bulk holes accordingly. In contrast, on the electron side the  $2 \cdot f_2^e(V_g)$  (cyan triangles) and  $f_3^e(V_g)$  (blue triangles) dependencies demonstrate different slope indicating to the different nature of the peaks characterized by these frequencies. Inset – the enhanced difference between hole  $(f_2^h - 2 \cdot f_1^h)/f_2^h$  (red circles) and electron  $(f_3^e - 2 \cdot f_2^e)/f_3^e$  (blue triangles) traces at the same values of  $V_g$ .

tained from SdH oscillations with the total density, obtained from Drude fits. An almost perfect coincidence of  $n_{\text{Drude}}(V_g)$  with  $n_{\text{top}} + n_{\text{bot}} + n_{\text{bulk}}$  is obtained (see Fig. 3 (e)). All other possible correspondences of Fourier peaks with groups of carriers were checked but much worse agreement in the relation  $n_{\text{Drude}} = e/h \cdot (\sum g_i f_i^e)$  was obtained, where  $g_i = 1, 2$  are possible spin degeneracies. An additional check that  $f_3^e \neq 2 \cdot f_2^e$  has been performed proving that the peaks with  $f_2^e$  and  $f_3^e$  frequencies have different origins. Indeed, as one could easily see in the Fig. 4 (b),  $f_3^e(V_g)$  and  $2 \cdot f_2^e(V_g)$  dependencies have different slopes with the interception around  $V_g = 10$  V indicating to their distinct origin.

Conclusively, the combined analysis of capacitance and

magnetotransport data allows to distinguish and identify three groups of electrons. An additional information about band structure could be obtained by linear extrapolation of  $n_{\text{bulk}}(V_g)$  dependence (Fig. 3 (e)). The cross-section with the horizontal axis occurs at  $V_g = 1.2$  V and marked  $E_C$  as a bottom of conduction band. The top of the valence band  $E_V$  was correctly determined by classical transport analysis and located at  $V_g = 0.8$  V. The difference between  $E_C$  and  $E_V$  defines the bulk energy gap. The obtained value of 0.4 V is 5 times smaller than was obtained in strained HgTe films [14, 16]. Therefore one could estimate that the energy gap value in partially relaxed HgTe film has the value of around 2-3 meV. One should not that the obtained energy gap value has the same order as the characteristic disorder in the system and so one could consider the system as a virtually gapless. Therefore we experimentally proved that the gap presence is not essential for the formation of spin non-degenerated surface states.

#### IV. CONCLUSION

In conclusion, by combining of transport measurements together with capacitance spectroscopy we have performed the analysis of the 200 nm partially relaxed HgTe film. The Drude fit of classical magnetotransport revealed the ambipolar electron-hole transport with high electron mobility. The detailed analysis of Shubnikov-de Haas oscillations both in conductivity and capacitance allowed to distinguish three groups of electrons identified as electrons on the top and bottom surfaces and the bulk electrons. The value of bulk energy gap is found to be experimentally indistinguishable from zero. It has been established that the absence of the gap does not affect to the main properties of the surface states which is found to be spin non-degenerate. The results of the work confirm that topological surface states are robust to the existence of trivial carriers. Presented techniques allows to investigate other 3D TIs regardless of the bulk gap or conductance existence.

#### ACKNOWLEDGMENTS

This work supported by RFBR Grants No. 18-32-00138 (transport results) and 18-42-543013 (together with the Government of the Novosibirsk Region of the Russian Federation). D.K. was supported by Russian

President grant MK-3603.2017.2.

#### Appendix: SdH-oscillations analysis

The analysis of Shubnikov-de Haas oscillations allows to determine the carriers density with rather high precision, but in the case of several types of carriers the procedure should be performed carefully. Here we describe how the oscillations were processed.

At the first step we measure the wide range magnetic field dependencies of the longitudinal  $\rho_{xx}$  and perpendicular  $\rho_{xy}$  components of resistivity tensor. Then we calculate an experimental conductivity trace  $\sigma_{xx}(B^{-1})$ , with which it is better to process than  $\rho_{xx}$  because of smaller monotonous part but which still has to be removed. The monotonous part, denoted as  $\langle \sigma_{xx} \rangle$ , was obtained by smoothing of every  $\sigma_{xx}(B^{-1})$  trace with the averaging period higher than the characteristic oscillations period. Finally the oscillatory conductivity part was normalized using the formula  $\Delta\sigma_{xx}/\sigma_{xx}^0 = (\sigma_{xx}(B^{-1}) - \langle \sigma_{xx}(B^{-1}) \rangle) / \sigma_{xx}(B = 0)$  and shown in the Fig. 3 (a), (b). The last step before Fourier transform was the magnetic field range shrinking, because small fields does not consist any useful information while at high fields the transition to the quantum Hall state begins. On the hole side the optimal range was found to be from 1.1 T to 3 T, while on the electron side the range was limited from 0.2-0.4 to 1 T depending on the gate voltage. The maximum oscillations amplitude was of about 10-15%.

For the capacitance traces  $C(B)$  the procedure was rather similar. The only difference was absence of monotonous part so  $\Delta C(B^{-1}) = C(B^{-1}) - C(B = 0)$ . For the electron side the magnetic field range was limited from 0.3-0.4 to 1 T depending on the gate voltage. For the hole side the capacitance measurements were not performed.

Finally every oscillatory trace was subject to fast Fourier transform. The typical obtained spectra are shown in the Fig. 4 (a). Each spectrum demonstrates a set of peaks which are characterized by frequency of  $f_i$ . The best known way to determine the precise  $f_i$  value, especially in a case of closely spaced peaks, is to fit each peak with any dome-like dependence. We used Gaussian functions  $A_i \exp(-\frac{(f-f_i)^2}{2\Delta f^2})$  with a central frequency of  $f_i$  for fitting of each peak. The obtained fitting shown with solid lines in Fig. 4 (a) while the corresponding central frequencies are marked by the vertical arrows.

- 
- [1] Y. Ando, *J. Phys. Soc. Japan* **82**, 102001 (2013), [arXiv:1304.5693](#).
  - [2] Y. Fan and K. L. Wang, *SPIN* **06**, 1640001 (2016).
  - [3] J. Wiedenmann, E. Bocquillon, R. S. Deacon, S. Hartinger, O. Herrmann, T. M. Klapwijk, L. Maier, C. Ames, C. Brüne, C. Gould, A. Oiwa, K. Ishibashi,

S. Tarucha, H. Buhmann, and L. W. Molenkamp, *Nat. Commun.* **7**, 10303 (2016), [arXiv:1503.05591](#).

- [4] V. Dziom, A. Shuvaev, A. Pimenov, G. V. Astakhov, C. Ames, K. Bendias, J. Böttcher, G. Tkachov, E. M. Hankiewicz, C. Brüne, H. Buhmann, and L. W. Molenkamp, *Nat. Commun.* **8**, 15197 (2017),

- arXiv:1603.05482.
- [5] M. Sato and Y. Ando, *Reports Prog. Phys.* **80**, 076501 (2017).
  - [6] Y. Xia, D. Qian, D. Hsieh, L. Wray, A. Pal, H. Lin, A. Bansil, D. Grauer, Y. S. Hor, R. J. Cava, and M. Z. Hasan, *Nature Physics* **5**, 398 (2009).
  - [7] Z.-H. Pan, E. Vescovo, A. V. Fedorov, D. Gardner, Y. S. Lee, S. Chu, G. D. Gu, and T. Valla, *Phys. Rev. Lett.* **106**, 257004 (2011), arXiv:arXiv:1101.5615v2.
  - [8] O. Crauste, Y. Ohtsubo, P. Ballet, P. A. L. Delplace, D. Carpentier, C. Bouvier, T. Meunier, A. Taleb-Ibrahimi, and L. Levy, arXiv:1307.2008.
  - [9] C. Brune, C. X. Liu, E. G. Novik, E. M. Hankiewicz, H. Buhmann, Y. L. Chen, X. L. Qi, Z. X. Shen, S. C. Zhang, and L. W. Molenkamp, *Phys. Rev. Lett.* **106**, 126803 (2011).
  - [10] K. M. Dantscher, D. A. Kozlov, P. Olbrich, C. Zoth, P. Faltermeyer, M. Lindner, G. V. Budkin, S. A. Tarasenko, V. V. Bel'kov, Z. D. Kvon, N. N. Mikhailov, S. A. Dvoretzky, D. Weiss, B. Jenichen, and S. D. Ganichev, *Phys. Rev. B* **92**, 165314 (2015), arXiv:1503.06951.
  - [11] L. Wu, M. Salehi, N. Koirala, J. Moon, S. Oh, and N. P. Armitage, *Science* (80-. ). **354**, 1124 (2016).
  - [12] D. Culcer, *Phys. E* **44**, 860 (2012), arXiv:1108.3076.
  - [13] M. Brahlek, N. Koirala, N. Bansal, and S. Oh, *Solid State Commun.* **215-216**, 54 (2015), arXiv:1408.1614.
  - [14] D. A. Kozlov, Z. D. Kvon, E. B. Olshanetsky, N. N. Mikhailov, S. A. Dvoretzky, and D. Weiss, *Phys. Rev. Lett.* **112**, 196801 (2014).
  - [15] H. Maier, J. Ziegler, R. Fischer, D. Kozlov, Z. D. Kvon, N. Mikhailov, S. A. Dvoretzky, and D. Weiss, *Nat. Commun.* **8**, 2023 (2017), arXiv:1708.07766.
  - [16] D. A. Kozlov, D. Bauer, J. Ziegler, R. Fischer, M. L. Savchenko, Z. D. Kvon, N. N. Mikhailov, S. A. Dvoretzky, and D. Weiss, *Phys. Rev. Lett.* **116**, 166802 (2016), arXiv:1511.00606.
  - [17] J. Chen, H. J. Qin, F. Yang, J. Liu, T. Guan, F. M. Qu, G. H. Zhang, J. R. Shi, X. C. Xie, C. L. Yang, K. H. Wu, Y. Q. Li, and L. Lu, *Phys. Rev. Lett.* **105**, 176602 (2010).
  - [18] D. Kim, S. Cho, N. P. Butch, P. Syers, K. Kirshenbaum, S. Adam, J. Paglione, and M. S. Fuhrer, *Nature Physics* **8**, 460 (2012), arXiv:1105.1410.
  - [19] L. Bao, L. He, N. Meyer, X. Kou, P. Zhang, Z.-g. Chen, A. V. Fedorov, J. Zou, T. M. Riedemann, T. A. Lograsso, K. L. Wang, G. Tuttle, and F. Xiu, *Sci. Rep.* **2**, 726 (2012).
  - [20] S. Wolgast, Ç. Kurdak, K. Sun, J. W. Allen, D. J. Kim, and Z. Fisk, *Physical Review B - Condensed Matter and Materials Physics* **88**, 1 (2013), arXiv:1211.5104.
  - [21] P. Olbrich, L. E. Golub, T. Herrmann, S. N. Danilov, H. Plank, V. V. Bel'Kov, G. Mussler, C. Weyrich, C. M. Schneider, J. Kampmeier, D. Grützmacher, L. Plucin-ski, M. Eschbach, and S. D. Ganichev, *Physical Review Letters* **113**, 1 (2014), arXiv:1402.7173.
  - [22] J. Tian, C. Chang, H. Cao, K. He, X. Ma, Q. Xue, and Y. P. Chen, *Sci. Rep.* **4**, 4859 (2014).
  - [23] Y. Xu, I. Miotkowski, C. Liu, J. Tian, H. Nam, N. Ali-doust, J. Hu, C.-K. Shih, M. Z. Hasan, and Y. P. Chen, *Nat. Phys.* **10**, 956 (2014).
  - [24] R. Yoshimi, A. Tsukazaki, Y. Kozuka, J. Falson, K. S. Takahashi, J. G. Checkelsky, N. Nagaosa, M. Kawasaki, and Y. Tokura, *Nature Communications* **6**, 1 (2015), arXiv:1409.3326.
  - [25] C. Li, B. De Ronde, A. Nikitin, Y. Huang, M. S. Golden, A. De Visser, and A. Brinkman, *Physical Review B* **96**, 1 (2017), arXiv:1707.07011.
  - [26] J. Ziegler, R. Kozlovsky, C. Gorini, M.-H. Liu, S. Weishäupl, H. Maier, R. Fischer, D. A. Kozlov, Z. D. Kvon, N. Mikhailov, S. A. Dvoretzky, K. Richter, and D. Weiss, *Phys. Rev. B* **97**, 035157 (2018), arXiv:1708.07014.
  - [27] A. Shuvaev, G. Astakhov, C. Brüne, H. Buhmann, L. W. Molenkamp, and A. Pimenov, *Semiconductor Science and Technology* **27**, 124004 (2012).
  - [28] A. Shuvaev, A. Pimenov, G. V. Astakhov, M. Mühlbauer, C. Brüne, H. Buhmann, and L. W. Molenkamp, *Appl. Phys. Lett.* **102**, 241902 (2013), arXiv:1211.5569.
  - [29] J. Wiedenmann, E. Liebhaber, J. Kübert, E. Bocquillon, P. Burset, C. Ames, H. Buhmann, T. M. Klapwijk, and L. W. Molenkamp, *Physical Review B* **96**, 1 (2017), arXiv:1706.01638.
  - [30] L. Muchler, H. Zhang, S. Chadov, B. Yan, F. Casper, J. Kubler, S.-C. Zhang, and C. Felser, *Angew. Chemie Int. Ed.* **51**, 7221 (2012).
  - [31] B. Bradlyn, L. Elcoro, J. Cano, M. G. Vergniory, Z. Wang, C. Felser, M. I. Aroyo, and B. A. Bernevig, *Nature* **547**, 298 (2017), arXiv:1703.02050.
  - [32] N. Berchenko and M. Pashkovskii, *Physics-Uspekhi* **119**, 223 (1976).
  - [33] T. P. Smith, B. B. Goldberg, P. J. Stiles, and M. Heiblum, *Phys. Rev. B* **32**, 2696 (1985).
  - [34] Z. D. Kvon, E. B. Olshanetsky, D. A. Kozlov, N. N. Mikhailov, and S. A. Dvoretzky, *JETP Letters* **87**, 502 (2008).
  - [35] R. Fletcher, M. Tsaousidou, T. Smith, P. T. Coleridge, Z. R. Wasilewski, and Y. Feng, *Phys. Rev. B* **71**, 155310 (2005).
  - [36] A. Inhofer, S. Tchoumakov, B. A. Assaf, G. Fève, J. M. Berroir, V. Jouffrey, D. Carpentier, M. O. Goerbig, B. Plaçais, K. Bendias, D. M. Mahler, E. Bocquillon, R. Schlereth, C. Brüne, H. Buhmann, and L. W. Molenkamp, *Phys. Rev. B* **96**, 195104 (2017).
  - [37] E. E. Mendez, L. Esaki, and L. L. Chang, *Phys. Rev. Lett.* **55**, 2216 (1985).